Yb-induced (2×3) and (2×4) reconstructions on Si(100) studied by first-principles calculations and high-resolution core-level photoelectron spectroscopy

M. Kuzmin,[1,2,*] M. P. J. Punkkinen,[1] P. Laukkanen,[1,3] R. E. Perälä,[1] M. Ahola-Tuomi,[1]
T. Balasubramanian,[4] and I. J. Väyrynen[1]
[1]*Department of Physics, University of Turku, FIN-20014 Turku, Finland*
[2]*A. F. Ioffe Physico-Technical Institute, Russian Academy of Sciences, St. Petersburg 194021, Russian Federation*
[3]*Optoelectronics Research Centre, Tampere University of Technology, FIN-33101 Tampere, Finland*
[4]*MAX-lab, Lund University, SE-221 00 Lund, Sweden*
(Received 28 March 2008; published 21 July 2008)

We report here a combined theoretical and experimental study of Yb/Si(100)−(2×3) and −(2×4) reconstructions by means of first-principles calculations and high-resolution core-level photoelectron spectroscopy. Energetically stable atomic structures are presented for these reconstructions. Yb atoms are found to occupy the cave sites in the structures, and the Si substrate is strongly rearranged due to Yb adsorption. It is shown that scanning tunneling microscopy images and surface core-level shifts (SCLSs) calculated for these atomic configurations agree with experimental data, giving further support to the models. In addition, by comparing our theoretical and experimental Si 2*p* results, we discuss and interpret the atomic origins of SCLSs measured for the YbSi(100)−(2×3)/(2×4). Finally, the results presented are helpful in the analysis of (2×3) and (2×4) structures induced by other rare earth metals on Si(100).

DOI: 10.1103/PhysRevB.78.045318 PACS number(s): 68.35.−p, 68.37.Ef, 73.20.−r, 79.60.−i

I. INTRODUCTION

Recently, the growth of rare earth (RE) metals on Si(100) and, in particular, the self-assembly of quasi-one-dimensional (1D) RE silicide nanowires (NWs) has attracted a lot of interest due to their highly anisotropic electronic and structural properties, as well as technological importance for future applications.[1–3] In general, it has been found that the 1D RE silicide NWs coexist with a two-dimensional (2D) reconstruction layer, which is stabilized by the RE adsorption on the Si(100) substrate.[3,4] Therefore, such reconstructions can play a critical role in the RE silicide formation on Si(100), and the knowledge of their atomic and electronic structures is important to understand the physical mechanisms behind the 1D silicide growth and to control this growth.

Among the 2D RE/Si(100) reconstructions reported so far, the most typical phases are the (2×3) and (2×4) ones. The former phase has been observed for Yb,[5,6] Nd,[5] Er,[7] Eu,[8] and Sm (Ref. 9) and the latter for Dy,[10] Ho,[4] Yb,[5,6] and Nd (Ref. 5). A recent scanning tunneling microscopy (STM) and first-principles calculation study, which was focused on the Gd/Si(100) system,[11] has shown that the (2×3) and (2×4) structures can be considered as building blocks for more complicated (2×7) and (2×8) reconstructions. Hence, the detailed information about the RE-induced (2×3) and (2×4) structures on Si(100) is essential for understanding of the RE/Si(100) systems. Due to complete filling of the 4*f* subshell, Yb($4f^{14}$) is known to be less reactive than other REs, and therefore, the critical metal coverage required for the onset of silicide formation in the RE/Si(100) system is expected to be higher for Yb than for other REs. Thus, the Yb/Si(100) represents a good platform for studying 2D structures.

In the low coverage regime [<0.3 monolayer (ML)], Yb has been reported to induce both the (2×3) and (2×4) periodicities on Si(100).[5,6] Low-energy electron diffraction (LEED) showed that the (2×3) periodicity found at 0.1–0.2 ML gradually changes to the (2×4) periodicity with increasing coverage.[5] STM revealed that the (2×3) and (2×4) phases are microscopically mixed and very related to each other: in empty-state images they show up rows of grouped oval protrusions, with two and three ones in each group, respectively.[5,6] A closer inspection of STM images indicated that the neighboring protrusions in both (2×3) and (2×4) unit cells are not identical in brightness and shape, and that the Yb atoms have two different bonding sites in each of the (2×3) and (2×4) phases. Although the registry of STM protrusions with respect to the surround clean Si(100) dimers has been clearly established,[5] the atomic structure of the (2×3) and (2×4) phases still remains unresolved. The STM images of the Yb/Si(100)(2×3)/(2×4) have been found to be strongly bias dependent, and thus they are not determined only by geometric effects, but also include a convolution of electronic effects. Therefore, interpretation of STM observations calls for theoretical support and, in particular, simulating STM images, which have not been so far reported for the RE/Si(100) reconstructions.

On the basis of Si 2*p* core-level photoemission, five surface core-level shifts (SCLSs) have been identified for the Yb-induced (2×3)/(2×4) reconstruction on a vicinal Si(100) substrate at 0.2 ML in Ref. 12. According to STM, this surface showed, in addition to the (2×3) and (2×4), some other structure (labeled *A* in Fig. 2 of Ref. 12), which was located near to the step edges and was different from the (2×3) and (2×4) phases. The origin of this structure was not clarified by STM, and therefore, unambiguous interpretation of SCLSs measured in Ref. 12 is complicated. Thus, Si 2*p* core-level shifts for the (2×3) and (2×4) reconstructions are still an open issue, and reinvestigation of Si 2*p* line shape for the well-defined (2×3)/(2×4) surface and comparison of experimental Si 2*p* data with theoretical calcula-

tions are required for better understanding of the (2×3) and (2×4) structures. To our knowledge, no Si $2p$ core-level calculations have been so far reported for the RE/Si(100) systems.

To address these unanswered questions, we have performed first-principles calculations to investigate the atomic geometries of Yb/Si(100)$-(2\times3)$ and $-(2\times4)$ reconstructions in detail. The results presented in this paper contribute to better understanding of the Yb/Si(100)$-(2\times3)/(2\times4)$ system as follows. (1) Based on our first-principles calculations, we report energetically favored atomic configurations with the bond lengths for the (2×3) and (2×4) phases. (2) Comparing our calculated STM images (in both empty and filled states) with the previously measured STM images in Refs. 5, 6, and 12, we find most likely atomic models for the (2×3) and (2×4) reconstructions. (3) Comparison of our calculated and measured Si $2p$ core-level shifts further supports these models and also clarifies the atomic origins of Si $2p$ components. Thus, the presented results provide a good ground for interpretation of STM images and Si $2p$ spectra for RE/Si(100)$-(2\times3)$ and $-(2\times4)$ surfaces in general.

II. EXPERIMENT

The measurements were performed on beamline 33 connected to the MAX-I storage ring at the MAX-lab in Lund, Sweden. The photoelectron spectra were taken with different photon energies (hv) and emission angles (θ_e) at RT under the residual pressure of about 4×10^{-11} Torr. The photon incidence angle was fixed at 45° from the surface normal. The overall energy resolution was around 100 meV increasing slightly with hv. The angular resolution was $\pm2°$. The binding energy was referred to the Fermi level.

The Si samples were cut from P-doped (n-type) (100) wafer (the surface misorientation was $\leq0.25°$). The samples were outgassed *in situ* at 873 K for several hours, followed by subsequent rapid flashings at 1473 K to remove surface oxide and carbon contaminations. After the cleaning, the well-ordered double-domain (2×1) LEED pattern with sharp half-order spots was found, and Si $2p$ core-level and valence-band spectra (not shown) exhibited pronounced features originating from the buckled dimers on the Si(100)(2×1) surface. The sample heating was performed by direct current. Temperature was measured by an infrared pyrometer. Ytterbium was evaporated from a tungsten-filament source. During the Yb deposition, the Si(100) substrate was held at RT, followed by post annealing at 850–900 K for several minutes to produce the long-range order. The Yb coverage for the $(2\times3)/(2\times4)$ surface was optimized by using LEED. The optimum value was taken slightly below the Yb coverage at which LEED features of the higher-coverage (2×6) reconstruction[5,6] appeared. In addition, our valence-band spectra taken for the $(2\times3)/(2\times4)$ surface at the optimized Yb coverage (not shown) indicated no sign of the Si-dimer-related peaks originating from the clean (2×1) reconstructed Si areas. Thus, the Si $2p$ spectra shown below are expected to be contributed by only the $(2\times3)/(2\times4)$ reconstruction. As in our previous study (Ref. 6), the quartz-crystal oscillator gave a coverage estimation of ~0.25 ML(1 ML$=6.78\times10^{14}$ atoms/cm^2) for this saturated $(2\times3)/(2\times4)$ surface. However, taking into account the above-mentioned LEED and valence-band observations and the atomic models shown below, we conclude that this coverage measured by the quartz-crystal oscillator is underestimated. The LEED pattern obtained for this surface is shown in Fig. 1. In this pattern, the (2×4) and (2×3) periodicities are manifested in the form of 1/4-order spots and 1/3-order stripes, respectively, agreeing with previous LEED observations.[6]

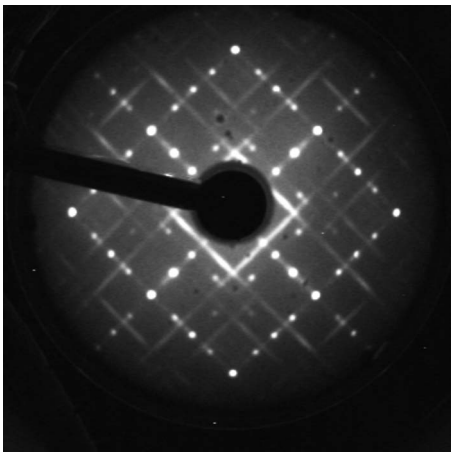

FIG. 1. LEED pattern of the Yb/Si(100)-$(2\times3)/(2\times4)$ surface. The electron energy is 61 eV.

III. CALCULATIONAL METHODS

The electronic structure calculations are performed using the *ab initio* total energy program VASP (Vienna *ab initio* simulation package),[13–16] which is based on the density functional theory.[17,18] Within this package the projector augmented wave (PAW) method[19,20] and the local density approximation (LDA) of Ceperley and Alder,[21] as parametrized by Perdew and Zunger,[22] are used. The optimization of the atomic structure is performed using conjugate-gradient minimization of the total energy with respect to the atomic coordinates. The Yb $6s$ and $5p$, and the Si $3s$ and $3p$ electrons are included as valence electrons. Slabs with 12 atomic layers (one Yb layer and eleven Si layers) are used. The dangling bonds of the bottom surface Si atoms are passivated by hydrogen atoms. Theoretical lattice constant (3.8387 Å) is used, and two bottom atomic layers of the slabs are fixed to the ideal positions. Other atoms, including the hydrogen atoms, are relaxed until the remaining forces are less than 20 meV/Å. The energy cutoff is 280 eV. The number of k points in the Brillouin zone is 24 (18) corresponding to a k mesh of $6\times4\times1(6\times3\times1)$ for $(2\times3)[(2\times4)]$ reconstructions. The surface core-level shifts within the initial-state model are evaluated by using the average electrostatic potential V_{atom} at the core of the Si atoms, which is obtained by placing a test charge (ρ_{test}) with the norm 1 at each Si ion and calculating[23]

$$V_{\text{atom}} = \int V(\vec{r})\rho_{\text{test}}(|\vec{r} - \vec{R}_n|)d^3\vec{r},$$

where the considered radius is 0.989 Å. The bulk reference value is obtained by averaging from different Si layers below fourth Si layer (two Si layers at the bottom surface are omitted[24]). Final-state shifts, calculated within complete-screening picture, include both initial-state shifts and final-state effects. In these calculations a single core electron is excited from the core to the valence by generating the corresponding core-excited PAW potential.[25] In the final-state calculations only the screening by valence electrons is included. It should be noted that the final-state values can be distorted, if (pseudo)hydrogenated slabs are used.[24] Therefore, final-state values are calculated only for (2×4) reconstructions by symmetrical (4×4) slabs. The constant-current STM images were simulated within the Tersoff-Hamann approximation,[26] in which the tunneling current is proportional to the energy-integrated local density of states.

IV. RESULTS AND DISCUSSION

A. Atomic models

On the basis of STM observations in Refs. 5 and 6, we consider several atomic structures for the Yb/Si(100)−(2×3) and −(2×4) reconstructions (Fig. 2) and test them theoretically. In all these models, the first-layer Si dimers, which are characteristic of the clean Si(100)−(2×1) surface, are assumed to be stripped off, as evidenced from earlier Si 2*p* study (Ref. 12), and the Si substrate initially has the bulk-terminated structure. For the (2×3) phase, the Yb coverage is proposed to be 1/3 ML in the both structures in Figs. 2(a) and 2(b), which corresponds well to the number of protrusions in empty-state STM images [two maxima per (2×3) unit] (Refs. 5 and 6). The Yb atoms are adsorbed at cave sites in Fig. 2(a) (the 2×3-I structure) and at valley-bridge sites in Fig. 2(b) (the 2×3-II structure) [note that bonding configurations for the two Yb atoms (i.e., Yb up and Yb down) in the (2×3) unit in Figs. 2(a) and 2(b) are not identical, as the STM protrusions are inequivalent[5,6]]. Likewise, the (2×4) models include three Yb atoms (the Yb triplet) per unit cell, where all Yb atoms are located either at cave sites [Figs. 2(c) and 2(d)] or at valley-bridge sites [Figs. 2(e) and 2(f)] (the 2×4-IA, 2×4-IB, 2×4-IIA, and 2×4-IIB structures, respectively). Two atoms of each Yb triplet are equivalent; they are associated either with bright STM protrusions in the "bright-protrusion-dark-protrusion-bright-protrusion" (BDB) configuration (the 2×4-IA and 2×4-IIA structures) or with dark STM protrusions in the DBD configuration (the 2×4-IB and 2×4-IIB structures).

The models of Fig. 2 were optimized by VASP. The fully relaxed atomic geometries of the above reconstructions are illustrated in Fig. 3. Our calculations indicate that both the (2×4)-IIA and (2×4)-IIB structures shown in Figs. 2(e) and 2(f) are unstable and converge to the same configuration given in Fig. 3(e). It will be called (2×4)-II hereafter. This behavior infers that the configurations with three Yb atoms adsorbed at valley-bridge sites are unstable. Instead, the (2×4)-II structure with two upper Yb atoms at caves sites and one lower Yb atom at valley-bridge site appears. The (2×3)-I and (2×4)-IA geometries with all Yb atoms at cave sites [Figs. 3(a) and 3(c)] are found to be the ground-state structures of the Yb/Si(100)−(2×3) and −(2×4) phases, respectively. The relative surface energies of the 2×3-I, 2×3-II, (2×4)-IA, (2×4)-IB, and (2×4)-II are shown in Table I. As seen, the surface energies of the (2×3)-I and (2×4)-IA are lower by 0.016 and 0.008 eV/(1×1) surface unit than those of the (2×3)-II and (2×4)-II, respectively. Therefore, the latter structures are the ground state ones for the (2×3) and (2×4) reconstructions, respectively.

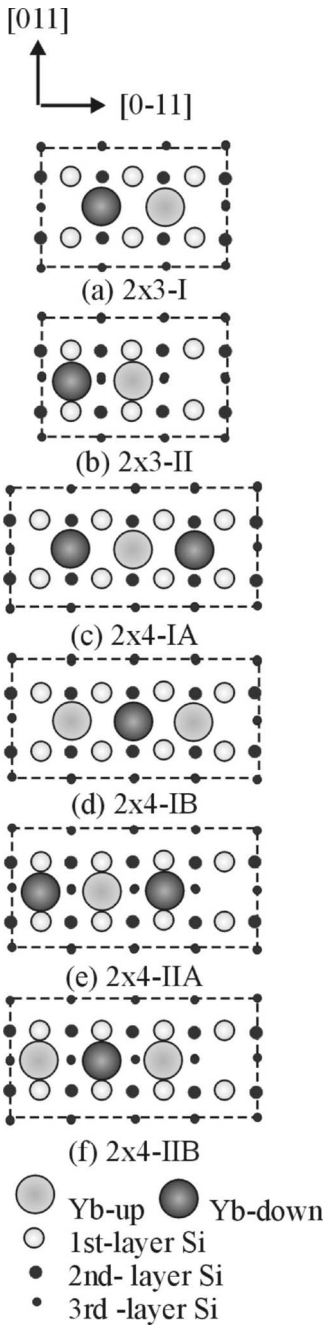

FIG. 2. Possible geometric structures (top view) of the Yb/Si(100)-(2×3) and-(2×4) phases. The (2×3) and (2×4) unit cells are shown by dot lines.

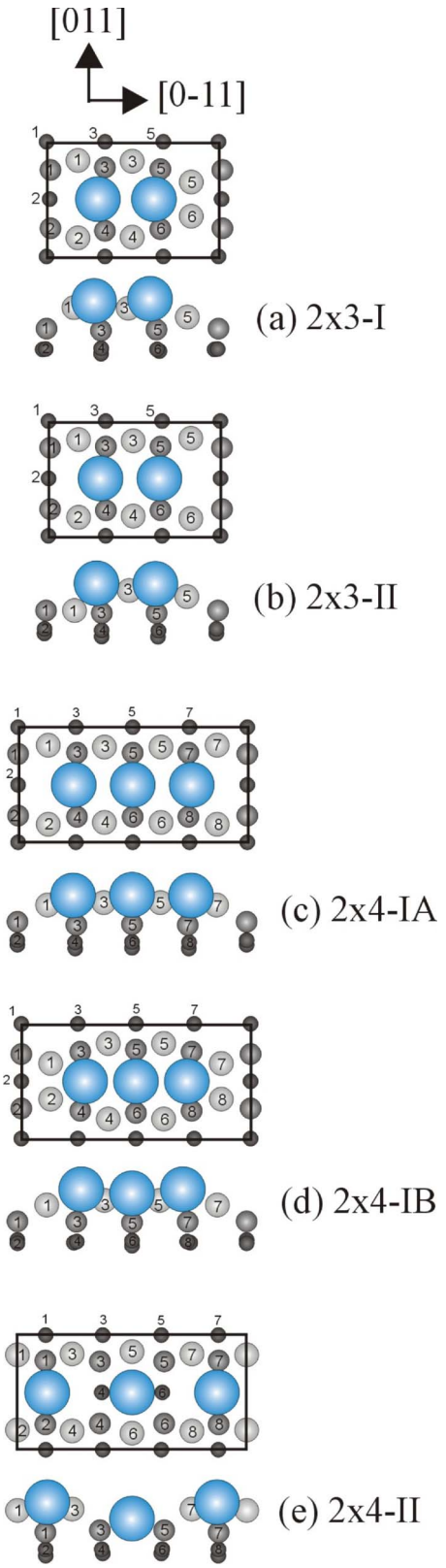

FIG. 3. (Color online) Fully optimized atomic models (top and side views) calculated for the Yb/Si(100)-(2×3) and-(2×4) reconstructions on the basis on the geometric structures in Fig. 2. The Yb atoms are shown by the large circles. Only three upper Si atomic layers are illustrated. The (2×3) and (2×4) are shown by line boxes.

TABLE I. Surface energy difference ΔE [eV/(1×1)] for the calculated models of Yb/Si(100)-(2×3) and-(2×4) reconstructions with respect to the ground-state (2×3)-I and (2×4)-IA structures, respectively.

	(2×3)-I	(2×3)-II	(2×4)-IA	(2×4)-IB	(2×4)-II
ΔE	0	0.016	0	0.058	0.008

A closer inspection of the atomic configurations in Fig. 3 gives more detailed information about the structural arrangement of the Yb/Si(100)-(2×3) and-(2×4) phases. Regarding the (2×3) phase, the following conclusions can be made. (1) The valley-bridge site is unfavorable for the Yb atoms in this structure. In both fully optimized (2×3)-I and (2×3)-II configurations, the equilibrium adsorption site for the Yb atoms is the cave one. Thus the (2×3)-II model of Fig. 2(b), where the Yb atoms are located at valley-bridge sites, is unstable; the optimization of this structure leads to the geometry [Fig. 3(b)] that is very similar to the (2×3)-I in Fig. 3(a). (2) The difference in height of two Yb atoms in the (2×3) unit for the models in Figs. 3(a) and 3(b) is 0.15 and 0.04 Å, respectively. Whereas the height difference of bright and dark STM protrusions in empty-state images is 0.34 Å (Ref. 6). Indeed, this is clear evidence that STM images of the Yb/Si(100)-(2×3) are strongly affected not only by geometric but also electronic structure effects, in good agreement with the finding that the images are bias dependent.[5] (3) In both the (2×3)-I and (2×3)-II structures, the first Si layer is strongly rearranged; the first-layer Si atoms tend to dimerize. There are three symmetrical (unbuckled) first-layer Si dimers [i.e., Si(1)-Si(2), Si(3)-Si(4), and Si(5)-Si(6) ones] per (2×3) unit. Furthermore, the bond lengths and vertical locations of such dimers are not identical. In particular, the bond lengths of the Si(5)-Si(6), Si(3)-Si(4), and Si(1)-Si(2) are 2.29, 2.60, and 2.49 Å in the (2×3)-I and 2.31, 2.64, and 2.48 Å in the (2×3)-II, respectively. The height differences of these dimers (along the [100] direction) are 0.64 and 0.59 Å for the (2×3)-I, and 1.34 and 0.93 Å for the (2×3)-II. In other words, one of these dimers [i.e., the Si(5)-Si(6) in (2×3)-I and the Si(1)-Si(2) in (2×3)-II] is significantly lower as compared to the other two dimers, and thus the dimer rows aligned along the [0–11] direction are modulated in height. Note that the [0–11] direction is parallel to the dimer row direction on the clean Si(100)-(2×1). (4) Moreover, the structure of underlying Si layers is also slightly modified, suggesting the Si rearrangement to penetrate deeply into the Si bulk. (5) The lateral separation of neighboring Yb atoms in a metal row of the (2×3)-I and –II is 3.75 and 3.94 Å, respectively. Taking the covalent radius of Yb (1.94 Å) into account, it is likely that the Yb atoms are able to interact directly to each other in these structures. In such a scenario an appearing of a vacancy between the Yb atoms paired in the [0–11] direction is thought to be responsible for the strain relief. The structural deformation in the first Si layer might have the same origin as well.

For the (2×4) structure, the cave site is also found to be favorable for all Yb atoms in the ground-state (2×4)-IA

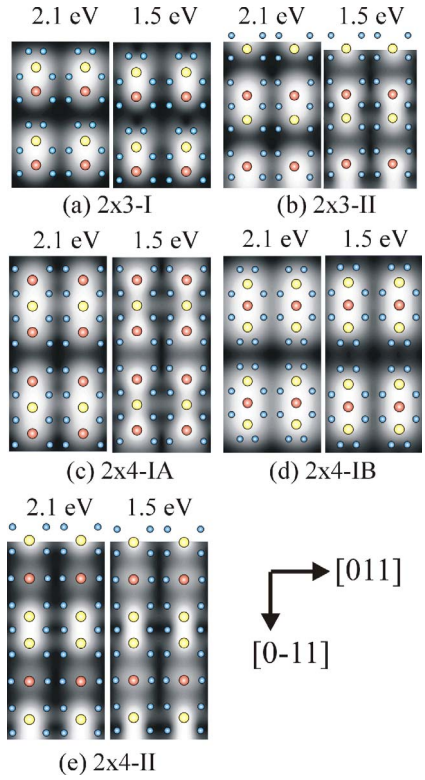

FIG. 4. (Color online) Simulated empty-state STM images for the (2×4)-I, (2×3)-II, (2×4)-IA, (2×4)-IB, and (2×4)-II structures in Fig. 3 within energy ranges of 2.1 and 1.5 eV above the calculated Fermi energy. The atomic positions of the Yb atoms and the first-layer Si atoms are given by large and small circles, respectively.

structure [Fig. 3(c)] and the related (2×4)-IB structure with reverse Yb-triplet configuration [Fig. 3(d)]. In the (2×4)-II structure, two atoms of the Yb triplet are adsorbed on cave sites, whereas the third Yb atom resides at the valley-bridge site [Fig. 3(e)]. For the (2×4)-IA and (2×4)-IB, the height differences between the outer and inner atoms of the Yb triplets are 0.05 and 0.27 Å, respectively, and the lateral separations of such atoms are 3.95 and 3.41 Å, respectively. Similar to the case of (2×3)-I and (2×3)-II structures, the first-layer Si atoms in the (2×4)-IA and (2×4)-IB form dimers, as shown in Figs. 3(c) and 3(d). In addition, the Si dimer rows of the (2×4)-IA and (2×4)-IB are aligned along the [0–11] direction, i.e., parallel to the Si dimer rows in the (2×3)-I and (2×3)-II. Obviously, this implies that the (2×3) and (2×4) structures with the Yb atoms at cave sites are closely related. In contrast, (2×4)-II [Fig. 2(e)] shows the height difference and lateral separation of the inner and outer Yb-triplet atoms to be much higher (1.10 and 5.68 Å, respectively).

B. STM

Figure 4 represents the spatial distributions of empty states for the (2×3)-I, (2×3)-II, (2×4)-IA, (2×4)-IB, and (2×4)-II configurations within energy ranges of 2.1 and 1.5 eV above the calculated Fermi energy. The equilibrium positions of Yb atoms and first-layer Si atoms in these configurations are also given for each structure. As the atomic arrangements of the (2×3)-I and (2×3)-II are shown to be very similar, it is not surprising that they give rise to similar empty-state distributions, where the most pronounced features (maxima) are located near to the Yb atoms, although the first-layer Si atoms are also seen to contribute to the above images. In particular, it means that the dangling bonds of first-layer Si atoms are not fully saturated by valence electrons donated by the Yb atoms to the Si substrate. In a simplified picture, two [three] Yb atoms, which are completely divalent in the (2×3) and (2×4) phases, as evidenced from Yb 4*f* measurements (not shown), can donate four [six] 6*s* electrons to the (2×3)[(2×4)] surface unit. Since these units include six and eight first-layer Si atoms with dangling bonds, respectively, it is obvious that all these dangling bonds cannot be completely saturated by the Yb adsorption in the (2×3) and (2×4) structures. More rigorously, the above STM images reflect the spatial distribution of electronic states induced by the covalent bonding of Yb and Si atoms in the (2×3) and (2×4) reconstructions.

More interestingly, the empty-state images of Fig. 4 are found to depend on bias voltage, in good agreement with experiment,[5] and the 1.5-eV images for the (2×3)-I and (2×3)-II structures are apparently different. Roughly, the (2×3)-II image shows two maxima centered on the Yb atoms and has the mirror-symmetry plane in the [011] direction (i.e., in the twofold-periodicity direction). In contrast, the (2×3)-I image shows, in addition to the two maxima caused by Yb, a pair of dim features located near to the Si(5) and Si(6) atoms, and therefore, it does not reveal the above mirror symmetry.

For the (2×4) models, the empty-state images are also bias dependent [Figs. 4(c)–4(e)]. It is worth noting that the main maxima are approximately centered on the Yb atoms, which is similar to the case of (2×3) models. However, the brightness of maxima does not always reflect the vertical position of Yb atoms. Especially, this trend is evident for the (2×4)-IA structure, where the 1.5-eV image shows the bright protrusions located on the lower Yb atoms and the dark protrusions located on the higher Yb atoms. In contrast, the higher the Yb atoms are located, the brighter the protrusions are in the 2.1-eV image. Thus the empty-state STM images calculated for both the (2×3) and (2×4) are bias dependent, giving support to experimental STM data in Ref. 5.

Filled-state STM images were simulated for the (2×3) and (2×4) structures at two bias voltages (−2.0 and –1.5 V). It is found that the filled-state images for each of the structural models are very similar at these bias voltages. For this reason, we present here only the ones calculated at –2.0 V (Fig. 5). As seen, they are rather different from the empty-state images in Fig. 4, thus supporting the aforementioned dependence of STM images on bias voltage. In particular, for the both (2×3)-I and -II structures, we note that the main contributions in the filled states are two unresolved bright protrusions located in the vicinity of the Yb atoms. In addition, a shoulder located near to the Si(5) and Si(6) atoms is seen. Obviously, the latter STM feature is slightly more evident in the case of the (2×3)-I structure. For the

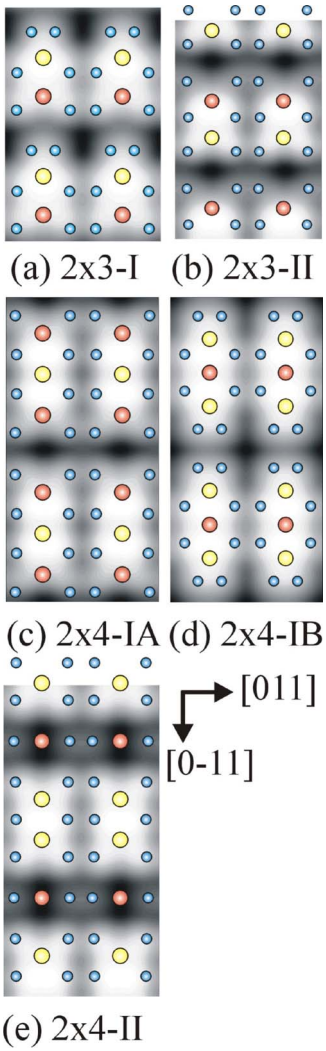

FIG. 5. (Color online) Simulated filled-state STM images for the (2×3)-I, (2×3)-II, (2×4)-IA, (2×4)-IB, and (2×4)-II structures (Fig. 3) within energy ranges of 2.0 eV below the calculated Fermi energy. See the other details in the caption of Fig. 4.

(2×4) structures, the main contributions to the filled-state images are also Yb atoms. Moreover, the first-layer Si atoms also provide a minor contribution. In general, the filled-state images exhibit lower contrast in brightness than the empty-state images, in good agreement with experimental STM results shown in Ref. 6.

To discriminate the atomic models for the (2×3) and (2×4) reconstructions, the calculated STM images in Figs. 4 and 5 are compared to the experimental ones obtained earlier in Refs. 5, 6, and 12. First, we notice that in experimental empty-state images, the contrast in brightness of different protrusions is found to depend on the bias voltage.[5] Obviously, this is consistent with the behavior of maxima in the calculated empty-state images of Fig. 4. Second, for the (2×3) reconstruction, some experimental empty-state images shown in Refs. 5 and 6 reveal two inequivalent maxima that exhibit not only different brightness but also different shape. This trend is rather consistent with the (2×3)-I structure rather than the (2×3)-II structure. In particular, the mirror symmetry considered above is clearly broken in the experimental images. In addition, the shape and location of protrusions in the empty-state images of Refs. 5, 6, and 12 reasonably agree with those of the calculated images for the (2×3)-I structure in Fig. 4(a). Third, the experimental filled-state images reveal the main bright protrusion, located in the vicinity of the bright maxima in the empty states, and the shoulder, located close to the position of the less bright protrusion in the empty states.[5] Clearly, this behavior is also consistent with our calculated images for the (2×3)-I structure in Fig. 4(a). We therefore conclude that the (2×3)-I model is the best candidate to describe the (2×3) phase, in good agreement with the surface-energy calculations showing this structure to be the ground state.

The experimental empty-state STM images of the (2×4) reconstruction show two types of unit cells, which include either one bright and two dark protrusions (the DBD triplet configuration) or one dark and two bright protrusions (the BDB one), and the protrusions exhibit an oval shape.[5,6,12] The calculated empty-state images for both the (2×4)-IA and (2×4)-IB in Figs. 4(c) and 4(d), respectively, reasonably reproduce these experimental observations. Furthermore, the filled-state images calculated for the above structures [Figs. 5(c) and 5(d)] are consistent with those in Ref. 5. In contrast, the STM images calculated for the (2×4)-II structure in the both empty and filled-state modes are fully inconsistent with the experimental images, and therefore, we rule out this structure as explanation of the (2×4) reconstruction. Thus, we assume that the (2×4)-IA and (2×4)-IB models are most plausible to account for the (2×4) phase. Note that according to our calculations, the ground-state structure of the (2×4) phase is the (2×4)-IA model (the BDB configuration) rather than the (2×4)-IB model (the DBD configuration), and the energy difference of these configurations is 0.058 eV/(1×1) (see Table I). However, the experimental STM images[5] clearly evidence that both the configurations equally coexist in spite of the above energy difference. Most likely, such behavior can be understood in terms of surface kinetics, which depends on the surface preparation and which were not taken into account in the above thermodynamic calculations.

C. Si 2*p* core level

To give further support to the atomic models suggested above, we calculated Si $2p$ core-level shifts for all the models in Fig. 3 [i.e., the (2×3)-I, (2×3)-II, (2×4)-IA, (2×4)-IB, and (2×4)-II], and compare these values with SCLSs in experiment. Theoretical values were obtained within both the initial-state and complete-screening (including both the initial- and final-state effects) models. The SCLSs calculated within the initial-state approach are given in Table II. Based on these calculations, the Si $2p$ core-level shifts are seen to occur for several atomic layers of the (2×3) and (2×4) (including the fourth and some deeper layers), and therefore, these reconstructions penetrate deeply enough into the bulk. The SCLSs calculated within the complete-screening model are found to be approximately the same as the initial-state SCLSs for the Si atoms in the second and deeper layers, and only for the first-layer Si atoms, the

TABLE II. Theoretical core-level shifts for Si atoms in the (2×3) and (2×4) reconstructions.

	Si(1)	Si(2)	Si(3)	Si(4)	Si(5)	Si(6)	Si(7)	Si(8)
				2×3-I				
1st layer	−0.36	−0.36	−0.04	−0.04	0.23	0.23		
2nd layer	0.12	0.12	−0.04	−0.04	0.28	0.28		
3rd layer	0.02	0.10	−0.17	0.29	0.21	0.31		
4th layer	−0.02	−0.08	−0.01	−0.04	−0.07	0.15		
				2×3-II				
1st layer	−0.10	−0.10	0.03	0.03	−0.42	−0.42		
2nd layer	−0.07	−0.07	0.19	0.19	0.02	0.02		
3rd layer	−0.21	0.28	0.00	0.40	−0.10	0.22		
4th layer	−0.28	0.20	−0.11	0.21	−0.26	0.13		
				2×4-IA				
1st layer	−0.20	−0.20	−0.18	−0.18	−0.18	−0.18	−0.20	−0.20
2nd layer	0.02	0.02	0.02	0.02	−0.04	−0.04	0.02	0.02
3rd layer	−0.06	0.22	−0.15	0.31	−0.13	0.31	−0.15	0.31
4th layer	−0.19	0.15	−0.24	0.18	−0.24	0.18	−0.19	0.15
				2×4-IB				
1st layer	−0.20	−0.20	−0.05	−0.05	−0.05	−0.05	−0.20	−0.20
2nd layer	0.15	0.15	0.09	0.09	0.08	0.08	0.09	0.09
3rd layer	0.27	−0.07	0.13	0.14	−0.04	0.34	0.13	0.14
4th layer	0.02	−0.02	0.01	−0.07	0.01	−0.07	0.02	−0.02
				2×4-II				
1st layer	−0.39	−0.39	−0.44	−0.44	0.04	0.04	−0.44	−0.44
2nd layer	−0.22	−0.22	−0.22	−0.22	0.20	0.20	0.20	0.20
3rd layer	−0.30	0.20	−0.31	0.20	−0.02	0.47	−0.02	0.47
4th layer	−0.34	0.07	−0.28	0.24	−0.08	0.38	−0.28	0.24

complete-screening SCLSs are somewhat different from the initial-state ones showing a clear tendency to move toward the lower binding energy as compared to the respective initial-state values. We note that this trend has been also observed for the clean Si(100)-(2×1) and Ge(100)-(2×1) surfaces.[27]

In general, the analysis of the results in Table II shows that the core-level shifts evaluated for different atomic structures are scattered approximately throughout the similar energy ranges. For example, the energy ranges for the (2×3)-I and (2×3)-II structures are –0.36 to 0.31 eV and –0.42 to 0.40 eV, respectively. Therefore, we cannot unambiguously discriminate between these models on the basis of calculated Si $2p$ core-level shifts; however, these results are important to test the validity of the suggested structural models by comparing the theoretical core-level shifts with those observed in experiment. As already mentioned in Sec. I, the core-level data measured for the Yb-stabilized (2×3)/(2×4) surface on the vicinal Si substrate in Ref. 12 are not suitable for such comparison. Hence, in this study we reexamine the Si $2p$ line shape for the Yb-induced (2×3)/(2×4) with the optimized metal coverage on the nominally flat Si(100) substrate (see Sec. II). Figure 6 shows Si $2p$ spectra taken for such a surface at $h\nu=135$ eV and $\theta_e=0°$ and 60°. The experimental data are given by open circles. The quantitative analysis of the spectra was done by using the standard fitting procedure with a linear combination of Voigt function peaks, as described elsewhere.[8,28] The fitting parameters are listed in Table III. As seen, the fitting results indicate the presence of four surface components $S1$-$S4$ with SCLSs of-0.43,-0.13, 0.21, and 0.39 eV relative to the bulk peak B for the (2×3)/(2×4) reconstruction. In Fig. 6, these are shown by shadowed doublets. The analysis of such data allows us to arrive at the following conclusions. (i) The Si $2p$ line shapes observed for the Yb/Si(100)-(2×3)/(2×4) surfaces in this study and Ref. 12 are different; the number of surface components found here is also different from that of Ref. 12. The present Si $2p$ data does not reproduce the lowest-binding-energy component with a core-level shift of –0.64 eV found in the case of the vicinal Si substrate ($S0$),[12] giving clear evidence that this component is not actually due to the (2×3) and (2×4) phases. In contrast, the other four surface components $S1$-$S4$ found for the vicinal Yb/Si surface in Ref. 12 are well reproduced in this study, indicating that these four SCLSs are indeed caused by the (2×3)/(2×4), and that the identical (2×3) and (2×4)

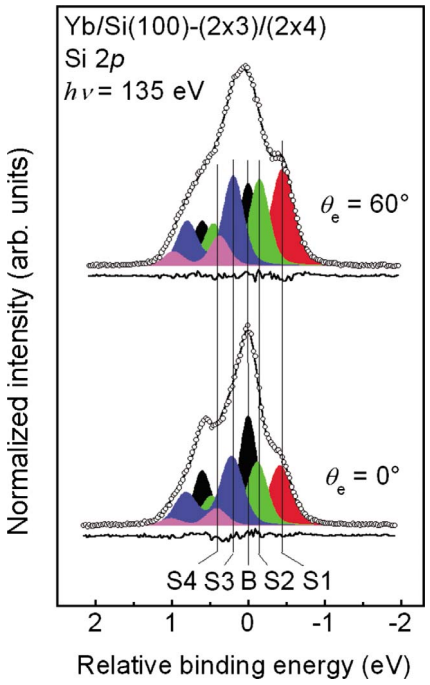

FIG. 6. (Color online) Si $2p$ core-level spectra for the Yb/Si(100)-$(2\times3)/(2\times4)$ surface at $h\nu=135$ eV and $\theta_e=0°$ and 60°. The raw data (open circles) are shown after the background correction by the Shirley's method. The fitting curves are given by solid lines. The residuals are shown for each spectrum by solid line. The bulk (B) and surface ($S1$, $S2$, $S3$, and $S4$) components are illustrated by shadow doublets.

structures can be formed by Yb on both flat and vicinal Si(100) surfaces. (ii) Comparison of the Si $2p$ results for the Yb/Si(100)-$(2\times3)/(2\times4)$ surface and the clean Si(100)-(2×1) surface (not shown) reveals that the bulk peak moves toward the higher binding energy by 0.12 ± 0.02 eV upon the Yb adsorption. Obviously, this infers that for the Yb-induced $(2\times3)/(2\times4)$, the Fermi level position in the band gap is moved upward by 0.12 eV as compared to the clean surface. Note that such behavior strongly resembles that of the Eu/Si(100)-(2×3) surface, where the respective value was found to be 0.14 eV.[8] (iii) Comparison of calculated core-level shifts in Table II with the measured data indicates a good agreement between these results, giving rise to further support for the validity of the atomic models suggested in Sec. IV B. Although the core-level binding-energy difference between some individual Si atoms in the (2×3) and (2×4) is so small that it is impossible to resolve all SCLSs in experiment within the instrumental resolution used, we emphasize that the general trends observed here for the Si $2p$ spectra might be helpful for the interpretation of Si $2p$ results for the related RE/Si(100)-$(2\times3)/(2\times4)$ systems in the future studies.

The theoretical Si $2p$ results allow us to clarify also the atomic origins of SCLSs identified in the experiment. For the (2×3)-I, (2×4)-IA, and (2×4)-IB models, which are the most plausible candidates to describe the (2×3) and (2×4) phases, the first-layer Si atoms reveal the shifts in the range between –0.36 and 0.23 eV within the initial-state scheme. Taking into account also the above-mentioned behavior of core-level shifts for the topmost-layer Si atoms within the complete-screening model, we conclude that the first-layer Si atoms in the (2×3) and (2×4) contribute mostly to the $S1$ and $S2$ peaks in Fig. 6. (In addition, we note that the B and $S3$ peaks might also be contributed by these atoms partly.) Taking into account the fact that the Si $2p$ core-level shifts to the lower binding energy upon reaction with Yb,[29] and that the first-layer Si atoms are directly bonded to Yb atoms in the models of Fig. 3, the above assignment is reasonable.

Regarding the deeper Si atoms taking part in the formation of the (2×3) and (2×4) reconstructions, the initial-state model was found to be adequate enough to reproduce SCLSs, as mentioned before, and the second- and third-layer Si atoms are thought to contribute to the $S2$, $S3$, and $S4$, in addition to B, whereas the fourth-layer Si atoms are assumed to cause the $S2$, $S3$, and B (see Tables II and III).

V. SUMMARY AND CONCLUSION

The Yb/Si(100)-(2×3) and -(2×4) reconstructions have been studied by first-principles calculations and core-level photoemission measurements. The results indicate that the (2×3)-I, (2×4)-IA, and (2×4)-IB models are the most plausible candidates to describe the atomic structure of (2×3) and (2×4) reconstructions. Our calculations also show that the (2×3)-I and (2×4)-IA structures are the ground states, while the surface energy of the (2×4)-IB is higher than that of the (2×4)-IA by 0.058 eV/(1×1). In all these structures, the atomic positions of the Yb atoms are cave sites, and the first Si layer is rearranged to form dimers

TABLE III. Fitting parameters for the Si $2p$ spectra of the Yb/Si(100)-$(2\times3)/(2\times4)$ surface. The spin-orbit splitting, branching ratio, and Lorentzian width are identical for all components. The values of spin-orbit splitting, Lorentzian width, Gaussian widths, and surface core-level shifts are given in electronvolts.

	B	$S1$	$S2$	$S3$	$S4$
Spin-orbit splitting			0.602		
Branching ratio			0.50 ± 0.02		
Lorentzian width			0.085		
Gaussian width	0.227	0.299	0.264	0.287	0.262
Surface core-level shift		−0.43	−0.13	0.21	0.39

that are parallel to the original Si dimers on the clean Si(100)-(2×1) surface. The simulated STM images are obtained for the above structure models at both bias polarities and different bias voltages. The images are shown to be bias dependent, and their main features are due to the Yb atoms and centered on them. In addition, the first-layer Si atoms provide a minor contribution to such images. The calculated STM images of the (2×3)-I, (2×4)-IA, and (2×4)-IB reasonably reproduce the experimental STM images acquired for the (2×3) and (2×4) phases in earlier studies, giving support to these atomic configurations.

The Si $2p$ core-level shifts are calculated for the above models and compared to the reexamined Si $2p$ spectra of the Yb/Si(100)-$(2\times3)/(2\times4)$ surface with the optimized metal coverage. The measured Si $2p$ spectra include four SCLS components $S1$, $S2$, $S3$, and $S4$ shifted by –0.43, −0.13, 0.21, and 0.39 eV relative to the bulk emission, respectively. Within a limited experimental resolution, these measured shifts can be well reproduced by our theoretical calculations for the (2×3)-I, (2×4)-IA, and (2×4)-B, supporting the validity of these models. The atomic origins of the measured SCLSs are discussed and clarified. In particular, it is concluded that the first-layer Si atoms mainly contribute to the SCLS components with two lowest binding energies ($S1$ and $S2$), reflecting the fact that the Yb atoms donate $6s$ electrons to the Si substrate when interacting with the surface. The second- and third-layer Si atoms are assumed to contribute to the $S2$, $S3$, and $S4$ and the fourth-layer Si atoms to $S2$ and $S3$. Finally, it is found that the Fermi level position at the band gap for the Yb/Si(100)-$(2\times3)/(2\times4)$ surface moves upward by 0.12 eV as compared to that of the clean Si(100)-(2×1) surface.

ACKNOWLEDGMENTS

We are grateful to H. Ollila and the MAX-lab staff for technical assistance. The financial support by the Transnational Access to the Research Infrastructure Program (TARI) is kindly acknowledged. This work has been supported in part by the Academy of Finland Grant No. 122743 (P.L.).

*m.kuzmin@mail.ioffe.ru

[1] C. Preinesberger, S. Vandré, T. Kalka, and M. Dähne-Prietsch, J. Phys. D **31**, L43 (1998).
[2] Y. Chen, D. A. A. Ohlberg, G. Medeiros-Ribeiro, Y. A. Chang, and R. S. Williams, Appl. Phys. Lett. **76**, 4004 (2000).
[3] J. Nogami, B. Z. Liu, M. V. Katkov, C. Ohbuchi, and N. O. Birge, Phys. Rev. B **63**, 233305 (2001).
[4] C. Ohbuchi and J. Nogami, Phys. Rev. B **66**, 165323 (2002).
[5] M. V. Katkov and J. Nogami, Surf. Sci. **524**, 129 (2003).
[6] M. Kuzmin, R. E. Perälä, P. Laukkanen, R.-L. Vaara, M. A. Mittsev, and I. J. Väyrynen, Appl. Surf. Sci. **214**, 196 (2003).
[7] J. Yang, Q. Cai, X.-D. Wang, and R. Koch, Surf. Sci. **526**, 291 (2003).
[8] M. Kuzmin, R. E. Perälä, P. Laukkanen, and I. J. Väyrynen, Phys. Rev. B **72**, 085343 (2005).
[9] C. Ohbuchi and J. Nogami, Surf. Sci. **579**, 157 (2005).
[10] B. Z. Liu and J. Nogami, Surf. Sci. **488**, 399 (2001).
[11] B. C. Harrison, P. Ryan, and J. J. Boland, Surf. Sci. **582**, 79 (2005).
[12] R. E. Perälä, M. Kuzmin, P. Laukkanen, R.-L. Vaara, and I. J. Väyrynen, Surf. Sci. **584**, 8 (2005).
[13] G. Kresse and J. Hafner, Phys. Rev. B **47**, 558 (1993).
[14] G. Kresse and J. Hafner, Phys. Rev. B **49**, 14251 (1994).
[15] G. Kresse and J. Furthmüller, Comput. Mater. Sci. **6**, 15 (1996).
[16] G. Kresse and J. Furthmüller, Phys. Rev. B **54**, 11169 (1996).
[17] P. Hohenberg and W. Kohn, Phys. Rev. **136**, B864 (1964).
[18] W. Kohn and L. J. Sham, Phys. Rev. **140**, A1133 (1965).
[19] P. E. Blöchl, Phys. Rev. B **50**, 17953 (1994).
[20] G. Kresse and D. Joubert, Phys. Rev. B **59**, 1758 (1999).
[21] D. M. Ceperley and B. J. Alder, Phys. Rev. Lett. **45**, 566 (1980).
[22] J. P. Perdew and A. Zunger, Phys. Rev. B **23**, 5048 (1981).
[23] G. Kresse and J. Furthmüller, *Vienna ab initio Simulation Package, Users Guide* (University of Vienna, Vienna, 2007).
[24] M. P. J. Punkkinen, K. Kokko, L. Vitos, P. Laukkanen, E. Airiskallio, M. Ropo, M. Ahola-Tuomi, M. Kuzmin, I. J. Väyrynen, and B. Johansson, Phys. Rev. B **77**, 245302 (2008).
[25] L. Köhler and G. Kresse, Phys. Rev. B **70**, 165405 (2004).
[26] J. Tersoff and D. R. Hamann, Phys. Rev. Lett. **50**, 1998 (1983); J. Tersoff and D. R. Hamann, Phys. Rev. B **31**, 805 (1985).
[27] E. Pehlke and M. Scheffler, Phys. Rev. Lett. **71**, 2338 (1993).
[28] See, for example, M. Kuzmin, P. Laukkanen, R. E. Perälä, R.-L. Vaara, and I. J. Väyrynen, Phys. Rev. B **71**, 155334 (2005); M. Kuzmin, R. E. Perälä, P. Laukkanen, M. Ahola-Tuomi, and I. J. Väyrynen, *ibid.* **74**, 115320 (2006); M. Kuzmin, K. Schulte, P. Laukkanen, M. Ahola-Tuomi, R. E. Perälä, M. Adell, T. Balasubramanian, and I. J. Väyrynen, *ibid.* **75**, 165305 (2007).
[29] L. Braicovich, I. Abbati, C. Carbone, J. Nogami, and I. Lindau, Surf. Sci. **168**, 193 (1986).